





Applying Depth Distribution of Seismicity to Determine Thermo-Mechanical Properties of the Seismogenic Crust in Southern California: Comparing Lithotectonic Blocks

EGILL HAUSSON¹  and MEN-ANDRIN MEIER¹ 

Abstract—We analyze waveform-relocated seismicity (1981–2016) and other geophysical and geological datasets from 16 lithotectonic crustal blocks in southern California. We explore how earthquake depth histograms (EDH) are related to crustal strength, lithology, and temperature of the crust. First, we calculate relative EDHs to quantify the depth distribution of seismicity for each lithotectonic block. Second, we calculate depth profiles of maximum differential stress (“yield strength envelopes”, YSEs) using Byerlee’s law and a non-linear dislocation creep law. We use observed average heat flow values, strain rates, and states of stress to parameterize YSEs for five different crustal candidate lithologies in each lithotectonic block. We assume that seismicity ceases where the mechanical rock strength falls below a critical threshold level, and identify the YSE that best predicts the depth extent of seismicity in each block. The lithologies of the best matching YSEs are found to agree well with expectations from past tectonics: they are mostly quartz-dominated except for the feldspar-rich diorite lithologies in the Great Valley, the southernmost western Sierra Nevada, Inner Continental Borderland, and Rifted crust in the Salton Trough. Similarly, the inferred thermo-mechanical properties, including differential stress, lithology, and geotherms reflect the previously mapped tectonic variability between the 16 lithotectonic blocks. On average, the differential yield stress is smaller and peaks at a shallower depth in hotter and more quartz rich crust but is larger and peaks at greater depths for colder and predominantly diorite crust. The good agreement between the modeled YSEs, the EDHs and tectonic considerations suggests that EDHs indeed reflect long-term geophysical properties of the crust and can be used to infer thermo-mechanical properties at depth. In contrast, shallow seismicity may be more likely to reflect short-term strain transients from fluid flow or recent anthropogenic disturbances.

Key words: Earthquake depth histograms, yield strength envelopes, lithology, crustal temperature, crustal thermo-mechanics.

1. Introduction

We use available seismicity and other geophysical datasets to develop a new understanding of the thermo-mechanics, including differential yield stress and the geotherm, of the seismogenic part of the southern California crust. We focus on the thermo-mechanics of blocks rather than individual faults to put our results into the context of the lithotectonics of the southern California crust (Fig. 1). The current lithotectonic fabric of the crust was formed during large-scale crustal extension dating back as far as ~ 30 or 40 m.y. (e.g., Crouch and Suppe 1993; Chapman 2017). During this rifting, many blocks rotated and moved 10 s of kilometers relative to stable eastern North America plate, including the western Transverse Ranges that rotated clockwise more than 90° (Luyendyk et al. 1980).

We use a representation of this tectonic fabric to group the seismicity into the depth distributions within each lithotectonic belt or block as modified by Oskin et al. (2016) based on the work of previous investigators such as (Crouch and Suppe 1993) (Fig. 1). This spatially heterogeneous seismicity is mostly associated with long-term loading of major fault systems that constitute the Pacific-North America plate boundary, as well as significant release of tectonic strain along the boundary, which occurs in major mainshock–aftershock sequences (Hauksson et al. 2012). Secondary processes such as gravitational collapse of the high Sierra Nevada, mid-crustal delamination, or anthropogenic activity related to geothermal energy also cause a small fraction of the seismicity.

The depth distribution of southern California seismicity has been the subject of several previous

¹ Seismological Laboratory, Division of Geological and Planetary Sciences, California Institute of Technology, Pasadena, CA 91125, USA. E-mail: hauksson@caltech.edu; mmeier@caltech.edu

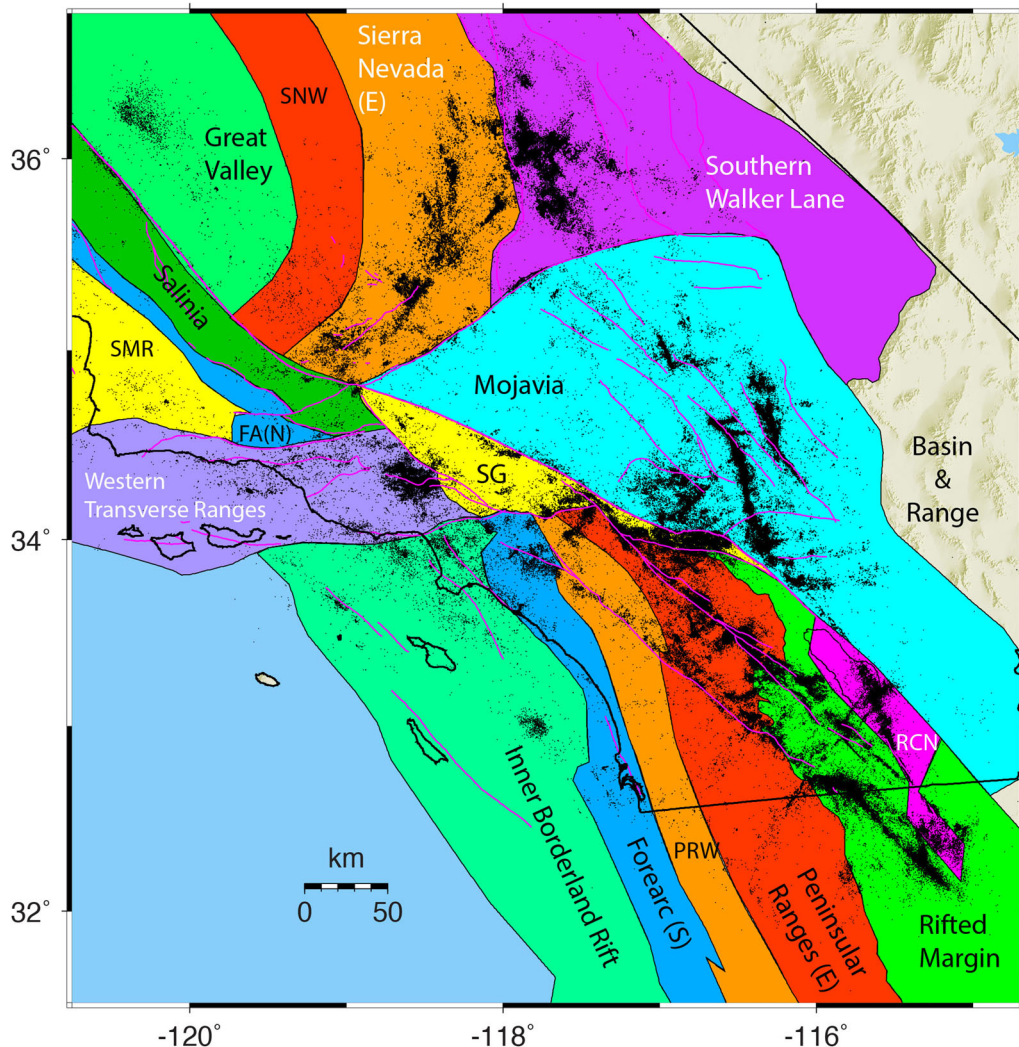


Figure 1

Map showing lithotectonic belts for southern California. Modified from Crouch and Suppe (1993) by Oskin et al. (2016). *PRW* Peninsular Ranges west, *SNW* Sierra Nevada west, *SMR* Santa Maria Rift, *FA(N)* Forearc north, *RCN* Rifted Crust north, *SG* San Gabriel. Waveform relocated hypocenter from Hauksson et al. (2012) and major faults from Jennings and Bryant (2010) are also shown. The block called “Rifted Crust south”, which is located outside southern California, has insufficient seismicity and thus is not included in this analysis. The basement of the Inner Continental Borderland rift consists of high-grade blueschist metamorphic rocks, which differ significantly from continental granite (Crouch and Suppe 1993). Both the Sierra Nevada and Peninsular batholiths have similar tectonic origin with quartz diorite, gabbro, and tonalite to the west (Chapman 2017). On the east side plutons with tonalite, granodiorite, and granite dominate. However, the arrangement of the lithotectonic belts in the southern Sierra Nevada no longer exists and batholith affinity assemblages dominate the region (Chapman 2017)

studies (Doser and Kanamori 1986; Magistrale and Zhou 1996; Williams 1996; Magistrale 2002; Bonner et al. 2003). They argued that varying combinations of lithology and temperature controlled the depth distribution of the seismicity. Nazareth and Hauksson (2004) used relocated seismicity to show that the seismogenic thickness ranged from 10 km in the

Salton Trough to 25 km beneath the southern Great Valley. They also inferred that the maximum moment release in moderate–large earthquakes extended to similar depths as the 99% moment release of the background seismicity, suggesting that the depth distribution of background seismicity is not magnitude dependent for ($M \leq 7.3$) southern California

mainshocks. In contrast, Rolandone et al. (2004) have used seismicity depth observations to suggest that the transient strain rate increase caused by the 1992 Mw7.3 Landers, California earthquake may have temporally increased the yield strength at depth, and led to seismic activity at depths that were aseismic without such perturbations.

Thermo-mechanical or rheology properties relate the response of crustal rocks to external forces under different pressure, temperature, and fluid content conditions. In the upper most 10–15 km, the mechanical strength of the crust is limited by the brittle rock strength, and can be described by Byerlee's law (Byerlee 1967). At greater depths, where the weakest minerals start to deform plastically, non-linear viscous creep laws can be used to describe the maximum strength (Sibson 1982; Albaric et al. 2009). Yield strength envelopes (YSEs) combine the two formulations to describe how the maximum mechanical strength varies with depth, where the overall yield strength is limited by the weaker of the two deformation mechanisms.

Besides strain rate and temperature, yield strength estimates are also primarily affected by the bulk rock composition and the style of deformation (Sibson 1984; Afonso and Ranalli 2004). In southern California, all four of these properties, including their lateral variations, are relatively well constrained from decades of high-quality geophysical (e.g., Hauksson 2011) and geological (e.g., Crouch and Suppe 1993; Chapman 2017) observations. This allows us to make well-informed predictions of how strength should change with depth in different places across southern California, and to compare them against observed seismicity.

Observed seismicity provides a direct observational constraint for lithospheric strength in that sufficient strength is a necessary, albeit not a sufficient, precondition for the occurrence of earthquakes. It provides information down to what depth level sufficient strength is present to store elastic strain energy. Previously, Déverchère et al. (2001) compared YSEs to EDHs from the Baikal rift system and estimated the thermo-mechanics of the seismogenic crust of predominantly mafic composition. Similarly, Albaric et al. (2009) analyzed YSEs and EDHs from the east African rift system. Both studies suggested

that by selecting the appropriate lithology and matching the shape of the EDHs and the YSEs they were able to determine local absolute differential stress depth profiles. There is, however, no clear physical motivation for why increased strength would result in higher seismicity, and hence we would not necessarily expect the YSEs and the EDHs to have the same shape. We, therefore, only make the much milder assumption that seismicity should be limited to depths where the YSE predicts substantial mechanical strength.

In each lithotectonic block, we make yield strength profile predictions for different candidate lithologies. We measure at what depths the strength decreases towards zero, and compare these estimates to the observed lower depth limit of seismicity. We explore to what extent the observed lateral changes in earthquake depths can be explained with changes in yield strength profiles and, in turn, to what extent seismicity observations can be used to constrain mechanical strength distributions at depth.

2. Lithotectonic Provinces

We use a lithotectonic model of southern California that divides the region into 16 lithotectonic provinces to group the seismicity (Fig. 1); (Oskin et al. 2016). This model identifies blocks by their lithotectonic assemblage of rocks, which have similar tectonic history. It draws heavily from the regional tectonic synthesis by Crouch and Suppe (1993) to delineate schist terranes, accretionary prisms, forearcs, rigid blocks, rifts, and batholiths. In particular, the forearc blocks were created by past tectonic processes such as arc-derived graywacke sedimentation on top, and scraped-off accretion from below. The western batholith belts (collision accretion), forearc belts (subsidence), and Santa Maria and Inner Borderland (Neogene rifting) have their own tectonic history and are characterized by their distinct lithology, ranging from quartz rich to feldspar rich, and geophysical properties such as heat flow (Crouch and Suppe 1993).

Some of the major late-Quaternary faults such as the SAF and the Garlock Fault form the major lithotectonic boundaries but a few of the model block

boundaries are preliminary such as the eastern boundary of Mojavia, which is a region of complex crustal deformation. It consists of attenuated batholith-derived crust underlain by Rand–Orocopia schist (Oskin et al. 2016). The northeastern boundary of Mojavia is based on Miller et al. (2000) but the eastern boundary and interior structure are highly uncertain. Its southeastern boundary is drawn to encompass most of schist outcrops described by Jacobson et al. (2011). Active from 12 Myr or later, the Southern Walker Lane in eastern California is a region of older lithospheric removal, and mantle upwelling characterized by several young volcanic rock fields, like Coso, and transtensional rifting (Oskin et al. 2016; Putirka et al. 2012). It also includes the Stateline Fault and crustal extension of Cretaceous granites and older rocks, which extends to the California–Nevada boundary in the east (Mahan et al. 2009).

Past subduction or rifting processes have added complexity to some of the lithotectonic blocks. Pelona schist underplates the shortened and deformed San Gabriel terraine that is bounded by San Andreas Fault, Sierra Madre Fault, and the Banning Fault (Matti and Morton 1993; and Oskin et al. 2016). The Rifted Crust north that floors the Salton Sea graben extends along the rift axis to the south across the Salton Sea, to about 30 km south of the US Mexico boarder. The Rifted Margin that extends across the western flank of the Salton Trough forms the edge of significant post-8 Ma transtensional rifting and highly attenuated continental crust on the margins of the Gulf of California (Oskin et al. 2016). The Pelona–Orocopia–Rand schist may be derived from shallow subduction complex (Chapman 2017).

3. Seismicity and Analytics

As part of our data analysis, we have reduced the southern and northern extents of the lithotectonic blocks to match the available seismicity distribution. Below we describe the datasets and the modeling approach used to determine the thermo-mechanical model of the crust.

3.1. Datasets

We analyze the relocated earthquake catalog from Hauksson et al. (2012), covering the time period from 1981 to 2016. We only include about 65% of the events that qualified for waveform cross-correlation and have high-quality hypocenters. Implicitly, we have excluded most of the $M > 4$ events because their waveforms do not cross-correlate with smaller events.

We determine a depth histogram for the whole dataset and for the seismicity of each individual block. We use 2-km-depth intervals to match the average uncertainties in the focal depths (Fig. 2). Implicitly, we assume that the number of earthquakes in each depth range is sufficient to determine a representative EDH.

We included aftershock sequences caused by the occurrence of a major mainshock, such as the 1992 Mw7.3 Landers, 1994 Mw6.7 Northridge, and Mw7.1 Hector Mine earthquakes, although these may have increased the cutoff depth by ~ 2 km, which is within the range of the depth uncertainty (Rolandone et al. 2004). Depending on the modeling approach, Beeler et al. (2018) showed that the coseismic deepening of slip is small or on the order of 10%, which would be 1–2 km in depth in this study. Thus, such changes in the depth of the 95%D would be within the depth uncertainties and are not easily detectable. If the frictional coefficient in the brittle regime is low, the coseismic deepening of the 95%D may be somewhat larger (Beeler et al. 2018). Ben-Zion and Lyakhovskiy (2006) performed 3D

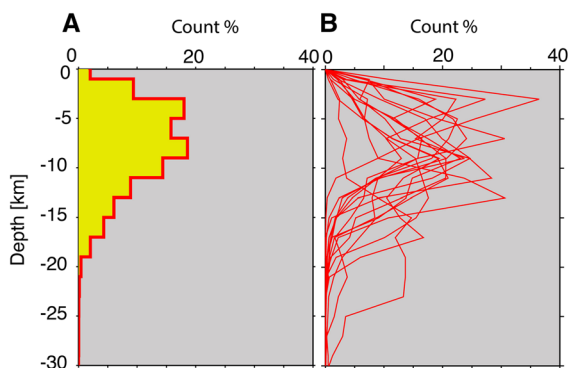


Figure 2
a Earthquake depth histogram (EDH) for the waveform relocated southern California (1981–2016) catalog of seismicity. **b** Average EDHs for each of the 16 lithotectonic blocks

numerical simulations in a model consisting of a seismogenic crust governed by viscoelastic damage rheology over a viscoelastic upper mantle. Their results show that mainshock ruptures can cause deepening of a small fraction of early aftershocks by ~ 5 km and up to 20 km in the cases considered. However, such cases of deep events are not observed in the aftershocks sequences of the analyzed 1981–2016 SCSN relocated catalog.

Using the method of Zaliapin and Ben-Zion (2013), we declustered the complete catalog (Hauksson et al. 2012) to isolate the effects of the long-term loading from short-term transient effects during aftershock sequences. However, the declustered catalog had almost identical EDHs for each block as the complete waveform relocated catalog, and so we proceed by the EDHs from the complete catalog.

We also determine the value of the geophysical parameters for each block by averaging values measured at each epicenter for: (1) USGS heat flow (C. Williams, written communication, 2016), (2) geodetic strain rate (Holt et al. 2010), and (3) style of faulting (Yang and Hauksson 2013), as shown in Fig. 3. To analyze the seismicity and the geophysical parameters, we determine the average value of each of these parameters for each block.

3.2. Determining Yield Strength Envelopes

A yield strength or yield stress is the material property defined as the stress at which a material begins to deform plastically. We use the empirical deformation laws for the brittle and ductile behavior of the crust to determine the peak differential stress as a function of depth (Sibson 1974, 1983).

3.2.1 Brittle Regime

Using modified Anderson theory, Sibson (1974) described the brittle behavior as Coulomb friction law that applies to favorably oriented existing faults when assuming negligible cohesion (less than 1 or 2 MPa):

$$(\sigma_1 - \sigma_3)(z) = \alpha \rho(z) g z (1 - \lambda), \quad (1)$$

where $(\sigma_1 - \sigma_3)$ is the difference between maximum and minimum principal stresses, ρ is average rock

density at depths shallower than z , α depends on faulting type and frictional coefficient, $\lambda \cong 0.4$ is the ratio of pore fluid pressure to overburden pressure, and g is the gravitational constant. The choice of the value of λ being hydrostatic is appropriate for strike-slip tectonic settings (Sibson 1984). The value of α depends on the style of faulting and has values of 3.0, 1.2, and 0.75 for thrust, strike-slip, and normal faulting (Afonso and Ranalli 2004). The average style of faulting within each lithotectonic block is determined using data from Yang and Hauksson (2013).

By Byerlee's law, we assume that the brittle crust is populated by randomly oriented faults within the stress field of each block. Byerlee's law is only experimentally verified to mid-crustal pressures but at higher pressures, the differential stress is no longer dependent on lithostatic load (Ranalli 1997).

3.2.2 Ductile Regime

At depth, we assume that the deformation of the ductile part of the crust consists of power law creep (dislocation recovery), which is highly temperature and composition dependent (Ranalli 1997). We use a power-law dislocation creep to model the ductile regime (Sibson 1983; Afonso and Ranalli 2004):

$$\sigma_1 - \sigma_3 = \left(\frac{\dot{\epsilon}}{A} \right)^{\frac{1}{n}} \exp \left(\frac{H}{nRT} \right), \quad (2)$$

$\dot{\epsilon}$ is the surface strain rate estimated from Holt et al. (2010), T is temperature in degrees Kelvin, R is universal gas constant. The creep parameters are n , A , and H , which is the creep activation enthalpy. The material parameters for the selected rock types are listed in Table 1. These parameters can easily vary by $\pm 25\%$ (Ranalli 1997).

The viscous creep parameters have been assigned mineral composition names, such as wet quartzite, quartz, granite, and quartz diorite. As discussed by Harden (1998) and in many other textbooks, these rocks can be described as follows. Quartzite was originally pure quartz sandstone and through heat and pressure was converted into metamorphic rock, which is characterized by low V_p and low Poisson's ratio. Granite is a coarse grained plutonic igneous rock that consists of 20–60% of quartz and at least 35% feldspar by volume. Diorite is an intrusive

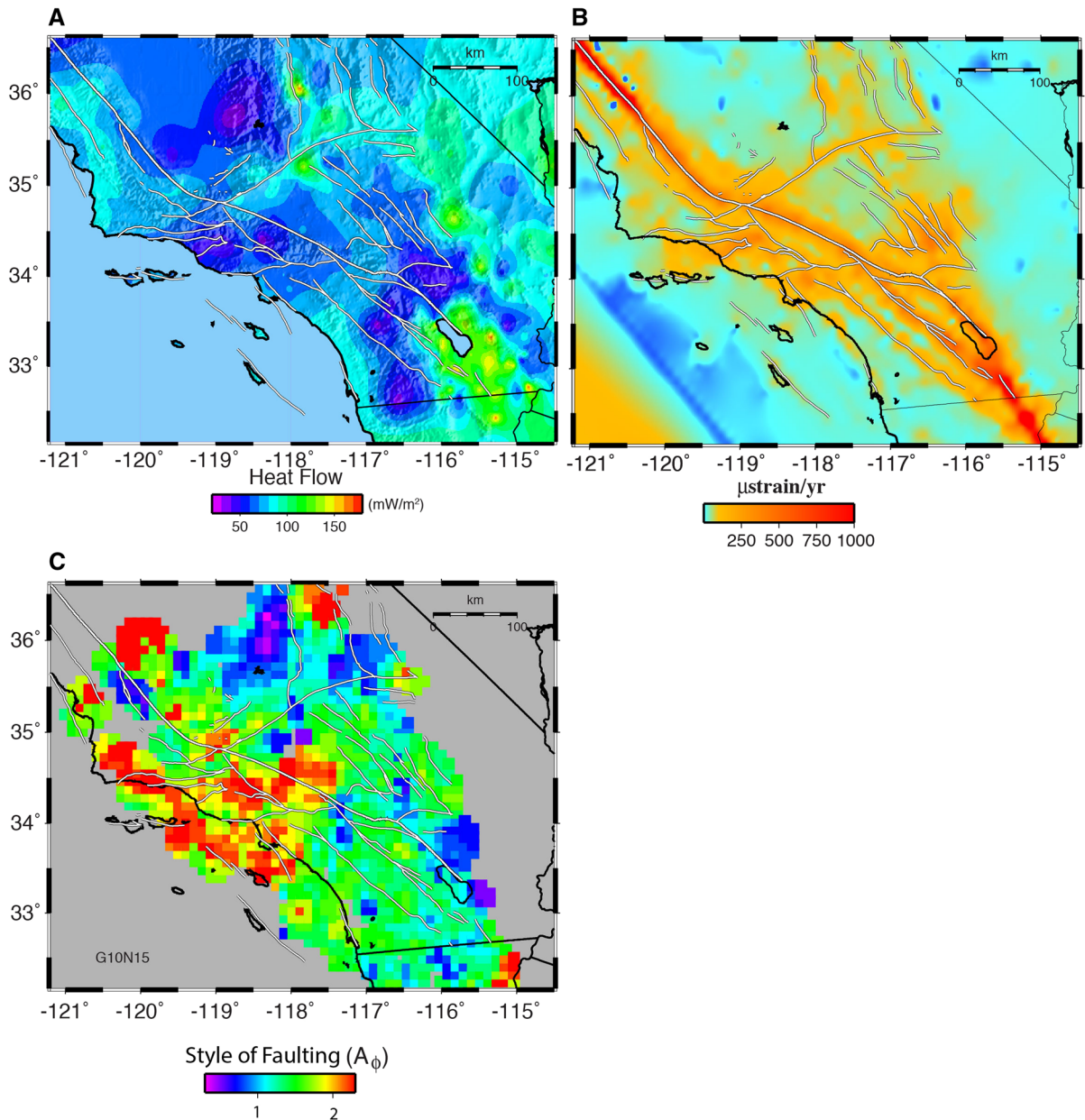


Figure 3

Southern California geophysical crustal parameters for **a** heat flow (C. Williams, written communication, 2016), **b** geodetic strain rate (Holt et al. 2010), and **c** style of faulting (Yang and Hauksson 2013)

batholithic igneous rock with a chemical composition that intermediates between gabbro and felsic granite. If diorite contains more than 5 wt% of quartz, it is generally referred to as quartz diorite but in this study, we are unable to resolve this difference. For completeness, we include parameters for a more

felsic rock, mafic granulite, in our analysis but our results indicate that felsic rocks are not present in significant quantities to affect our results. These choices agree with previously inferred crustal lithology profiles for the main physiographic provinces in California (Mooney and Weaver 1989).

Table 1

Viscous creep parameters and average crustal density as compiled by Ranalli (1997), Turcotte and Schubert (2002), Afonso and Ranalli (2004), and Albaric et al. (2009)

^a Mineral composition	A (MPa ⁻ⁿ s ⁻¹)	n	E (kJ mol ⁻¹)	Rho (kg m ⁻³)
Wet quartzite	3.2×10^{-4}	2.3	154	2640
Quartz	1.0×10^{-3}	2.0	167	2640
Granite	1.8×10^{-9}	3.2	123	2650
Quartz diorite	1.3×10^{-3}	2.4	219	2800
Mafic granulite	1.4×10^4	4.2	445	2880

^aSee text for explanation of A , n , E , and Rho

These designations of mineral composition should not be taken literally because the weakest of the most abundant minerals controls the mechanical properties of a rock (Burov 2011). In granite or quartzite, this is quartz, and poly-phase aggregate rocks are weaker than their constitutive minerals. For instance, adding micas to andesitic rocks lowers viscosity more than adding water (Shinevar et al. 2015). They also showed that the lower crustal viscosity of andesitic rocks (64 wt% quartz) was most consistent with rapid tectonic deformation processes such as post-seismic relaxation.

3.3. Determining Temperature Depth Profiles

Yield strengths generally vary strongly with temperature. We use the 1-D steady state heat conduction equation to determine the geotherm, $T(z)$ (Sass et al. 1997).

$$T(z) = T_0 + \left(\left(q - bA_0e^{-z/b} \right) z + b^2A_0(1 - e^{-z/b}) \right) / \lambda, \quad (3)$$

where z is depth in (km), T_0 is the surface temperature at 15 °C, A_0 is the surface value of heat production of $1.5 \mu\text{Wm}^{-3}$, b is assumed to be 15 km, λ is the thermal conductivity of $2.5 \text{Wm}^{-1}\text{K}^{-1}$, q is the surface heat flow (mWm^{-2}) which varies across southern California. The average heat flow values for each region are from the USGS database provided by C. F. Williams (*Written communication*, 2016). The assumed depth dependence of radiogenic heat production becomes less certain with depth, and the

crustal temperature may vary by several tens of degrees Celcius near the brittle ductile transition (Sass et al. 1997; Bonner et al. 2003).

3.4. Yield Stress Envelope (YSE)

The estimation of yield stress requires several assumptions because we know neither the true rheology nor the details of the applied tectonic strain field. To determine the yield stress profiles, we calculate the brittle and ductile yield stress as a function of depth using Eqs. (1), (2) and (3). The YSE at each depth is given by weaker of the two strength measures. This differential stress envelope depends on crustal density, stress state, heat flow, strain rate, and lithology, and describes the onset of brittle and ductile deformation in the material as a function of depth. In geodynamic applications, the differential stress envelopes are used to determine the strength of the whole crust by integrating the differential stress over the thickness of the crust (e.g., Afonso and Ranalli 2004).

To obtain relative strength envelopes of individual crustal blocks, we normalize the absolute YSEs by following Albaric et al. (2009) and integrate the differential stress in 2-km-depth increments, which corresponds to the average depth uncertainty of the seismicity, down to 30-km depth (Fig. 4). Because the area under the relative YSE curve is normalized, crust with a weak layer would exhibit a relative peak in the YSE at that depth, while a uniformly strong crust would exhibit a low amplitude YSE for the whole crustal thickness.

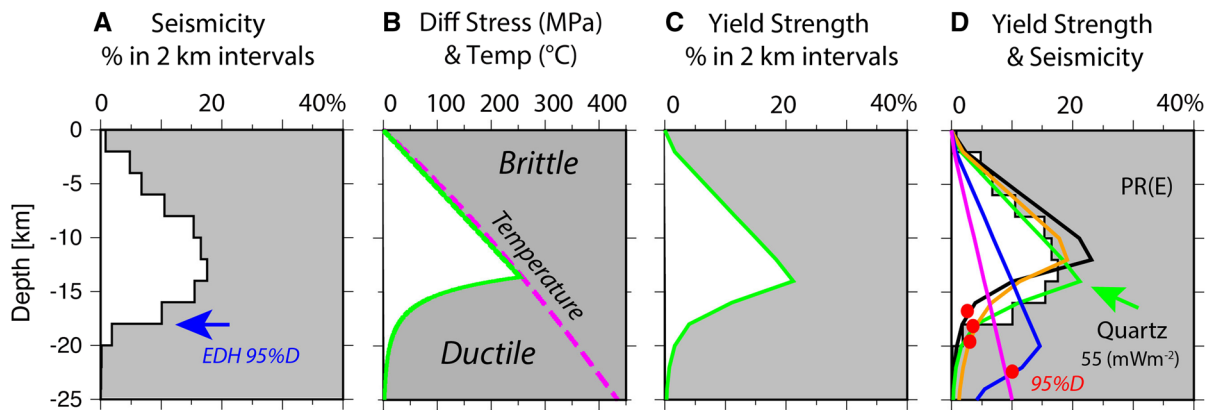


Figure 4

The four panels in this figure explain the data analysis method applied in this paper. **a** First we determine an earthquake depth histogram (EDH) and the 95% depth (95%D) shown as a blue arrow; **b** we calculate maximum differential stress and temperature depth profiles; **c** a sample integrated yield strength envelope (YSE) for quartz composition; and **d** comparison of the EDH and five YSEs for quartzite, granite, quartz, diorite, and mafic granulite. The 95% depth of each YSE is labeled with a red solid circle to facilitate comparison of the minimum distance of the EDH 95%D and the respective YSE 95%D. The 95%D of the quartz YSE has the best minimum distance fit to the EDH 95%D with heat flow of 55 mWm^{-2}

3.5. Effects of Crustal Properties on Relative YSEs

We selected a sample EDH for a region near the south end of the San Jacinto Fault to compare the effect of different crustal properties on the shape and depth offset of the corresponding relative YSEs (Fig. 5). We vary one of the four crustal parameters at a time within the expected range, while the other three are held fixed. Because the area under each yield curve is normalized, their peak value is inversely proportional to their total depth range. The heat flow and lithology have the strongest influence on the depth distribution of the YSEs, while the effects of the tectonic strain rate and style of faulting are less prominent. The three quartz-rich felsic compositions have similar YSEs (all other parameters being equal), which implies that we likely will not be able to distinguish between them with the resolution of our method.

4. Results

In this study we assume that the relative earthquake depth histogram (EDH) and the corresponding YSE for each lithotectonic block remain fairly stationary in space and time over centuries or longer. Thus, we can analyze them to infer the long-term

geophysics of the crustal blocks located adjacent to the plate boundary. These assumptions are in part supported by the Pacific and North America constant rate of relative strike-slip movement over the last several million years (Harden 1998; Chapman 2017).

4.1. Earthquake Depth Histograms (EDH)

In very general terms, the EDHs increase with depth, reaching a peak at different depths, and then decaying rapidly (Fig. 6). The rapid decay with depth is related to increasing temperature and associated onset of ductility. In this study, we use the 95% cutoff depth of the EDHs (95%D) as markers, because these are located in the depth range, where the crustal strength, stressing rate, and availability of nucleations converge to a minimum. This is justified for most of southern California where earthquakes are caused by plate boundary loading stress. However, it may not apply in limited areas that accommodate recent shallow-induced seismicity, located mostly in high heat flow geothermal areas (Hauksson et al. 2012). By calculating block averages, we implicitly assume that the lower crustal deformation under each crustal block is accommodated by distributed flow of viscous lower crust as opposed to localized ductile shear with associated localized changes in ductility and thermal

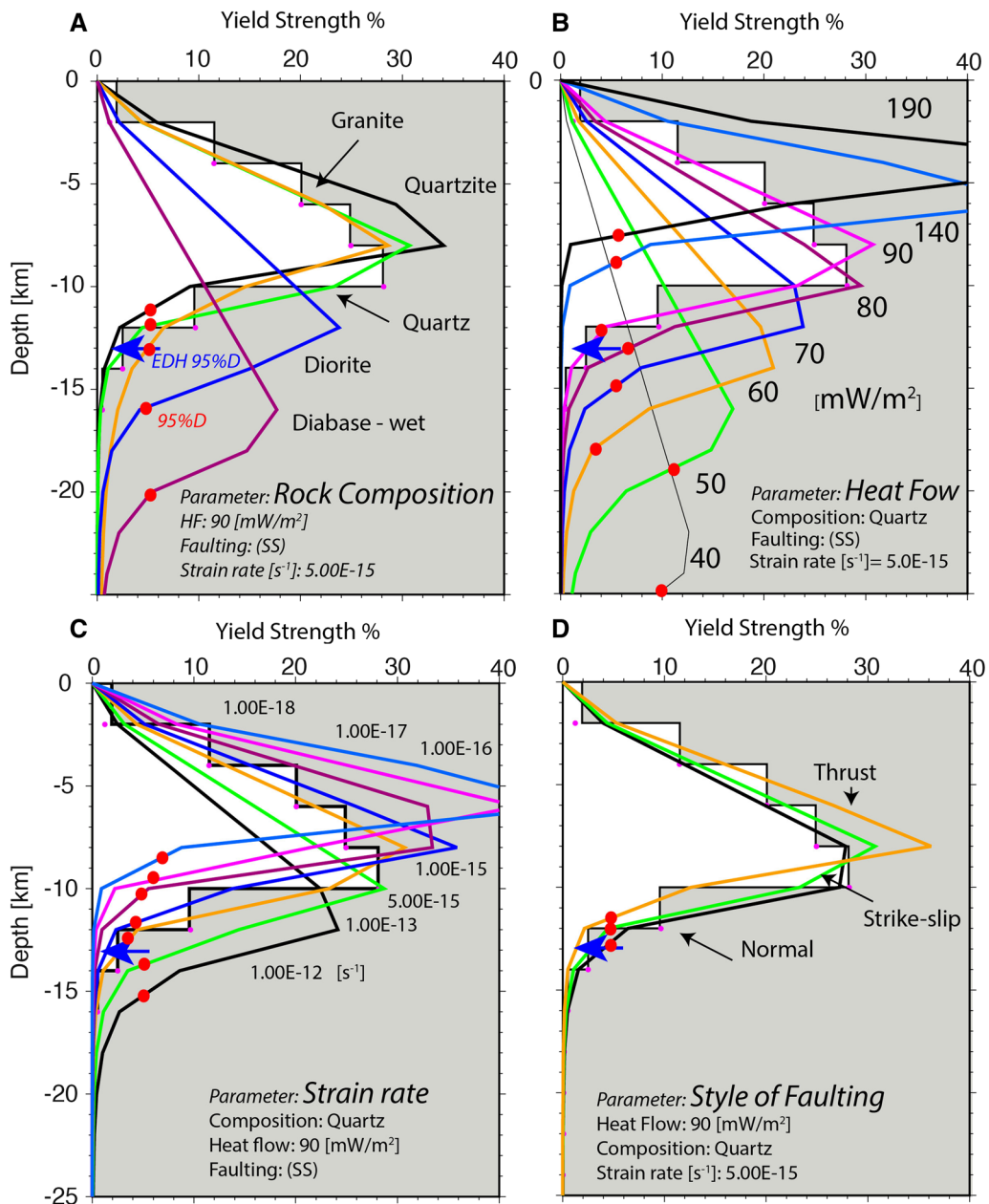


Figure 5

For a random earthquake depth histogram (EDH) with the 95% depth (95%D) shown as a blue arrow; we calculate the effects of the four geophysical parameters; **a** average lithology as labeled for different YSEs; SS—strike-slip faulting; **b** surface heat flow as labeled for different heat flow values; **c** surface GPS strain rate values and **d** styles of faulting as derived from the stress state. The 95% depth of each YSE is labeled with a red solid circle to facilitate comparison of the minimum distance of the EDH 95%D and the respective YSE 95%D

anomalies (Burgmann and Dresen 2008). In other words, we do not account for possible spatial variations in the ductile shear in the lower crust.

In four cases the EDHs appear to have double peaks (Fig. 6). These double peaks are likely caused

by superimposing distinct seismicity clusters in these blocks. The SG block, for instance, combines the 1994 Northridge earthquake sequence with the deep seismicity beneath the San Gorgonio region, where crustal delamination may play a role. These double

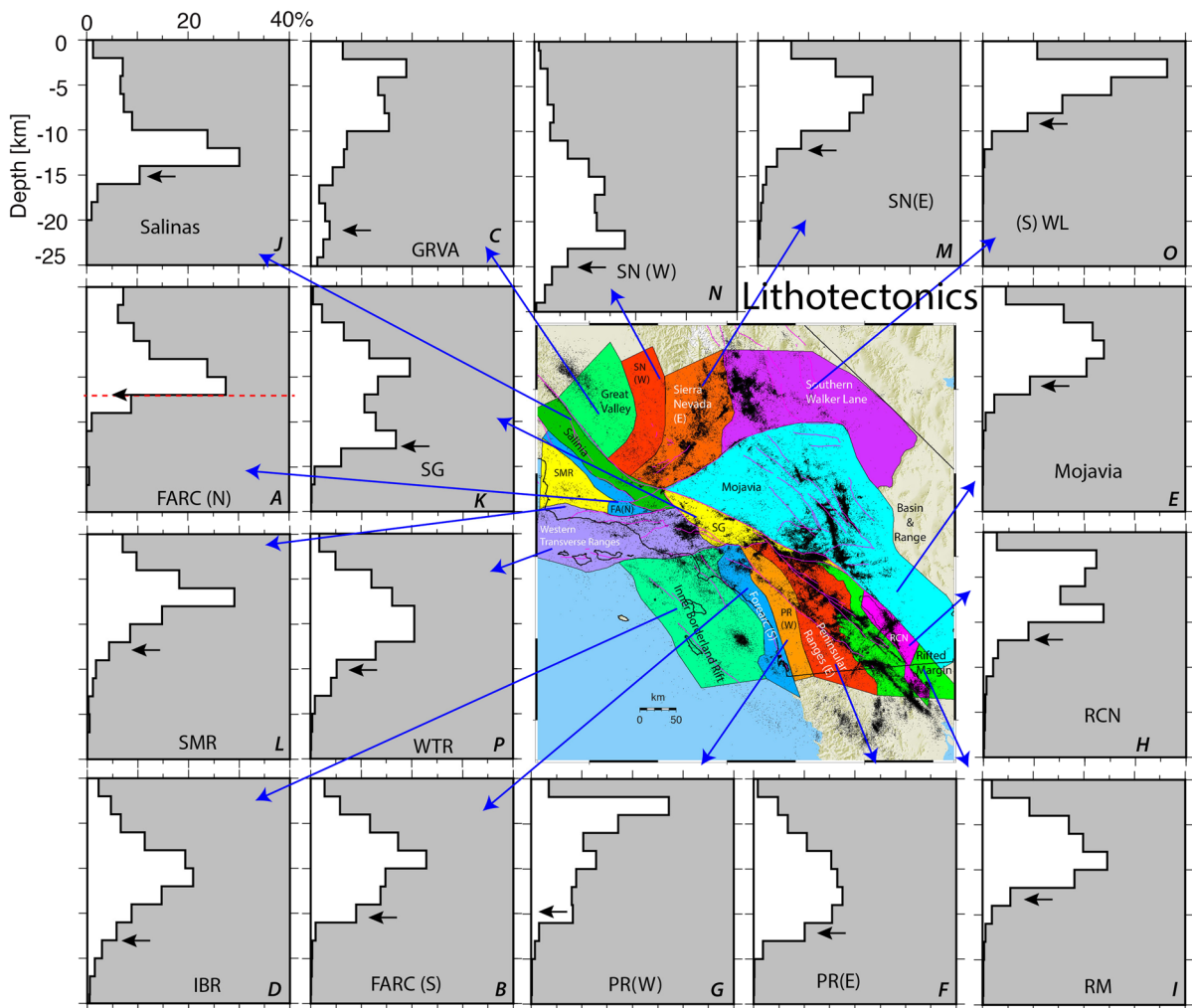


Figure 6

Relative earthquake depth histograms (EDH) for the 16 lithotectonic blocks ranging in depth from 0–25 or 30 km. The horizontal black arrows indicate 95% (95%D) seismicity depth. The blocks are labeled as: *GRVA* Great Valley, *SN (W)* Sierra Nevada (west), *SN (E)* Sierra Nevada (east), *(S) WL* south Walker Lane, *FARC (N)* Forearc (north), *SG* San Gabriel, *SMR* Santa Maria Rift, *WTR* Western Transverse Ranges, *RCN* Rifted Crust north, *IBR* Inner Continental Borderland, *FARC (S)* Forearc (south), *PR (W)* Peninsular Range (west), *PR (E)* Peninsular Range (east), *RM* rifted margin. The letter designation in each block also refers to Table 2

peaks are likely related to lateral variations within blocks but do not require depth-layered lithology or strength variations. In some cases, they may be related to different seismogenic processes, such as induced seismicity or complex plate boundary deformation such as crustal thickening. As an example, the deeper seismicity in the Rifted Crust north (RCN) was previously identified by Shearer (2002), as being more representative of the regional tectonic loading while most of the shallow seismicity is connected to geothermal processes. Most of the seismicity within

the Peninsular Range west (PRW) block is located in the northern part of the block. The deeper seismicity is located along the Elsinore Fault while the shallower part is to the north forming the Fontana seismicity trend (Hauksson et al. 2012).

In all 16 blocks we observe a dearth of seismicity at very shallow depths. Unless this is caused by systematic vertical location errors for very shallow events, this may indicate a velocity-strengthening friction regime, or the presence of aseismic deformation processes, such as solution-transfer.

4.2. Matching the Depth Extent of EDHs and YSEs (D95%)

The relative YSEs of the five possible lithologies calculated using the strain rate and heat flow for each lithotectonic block are shown in Fig. 7, along with the EDHs. In general, there are shape similarities between the EDHs and the YSEs with increasing values at shallow depth and decreasing values at greater depths. This similarity has prompted Déverchère et al. (2001) and Albaric et al. (2009) to assume that EDHs are directly proportional to the

YSE, i.e., that the number of earthquakes grows with yield strength. There is, however, no physical model that would predict such a relation.

Here, we make the much weaker assumption that seismicity should cease when the yield strength approaches zero. To this end, we determine the 95th percentile depths (“D95%”) for both EDHs and YSEs. For the EDHs the D95% is the depth at which 95% of events locate above. For the YSEs, D95% marks the depth at which 95% of the YSE function mass is above that depth. From the five candidate

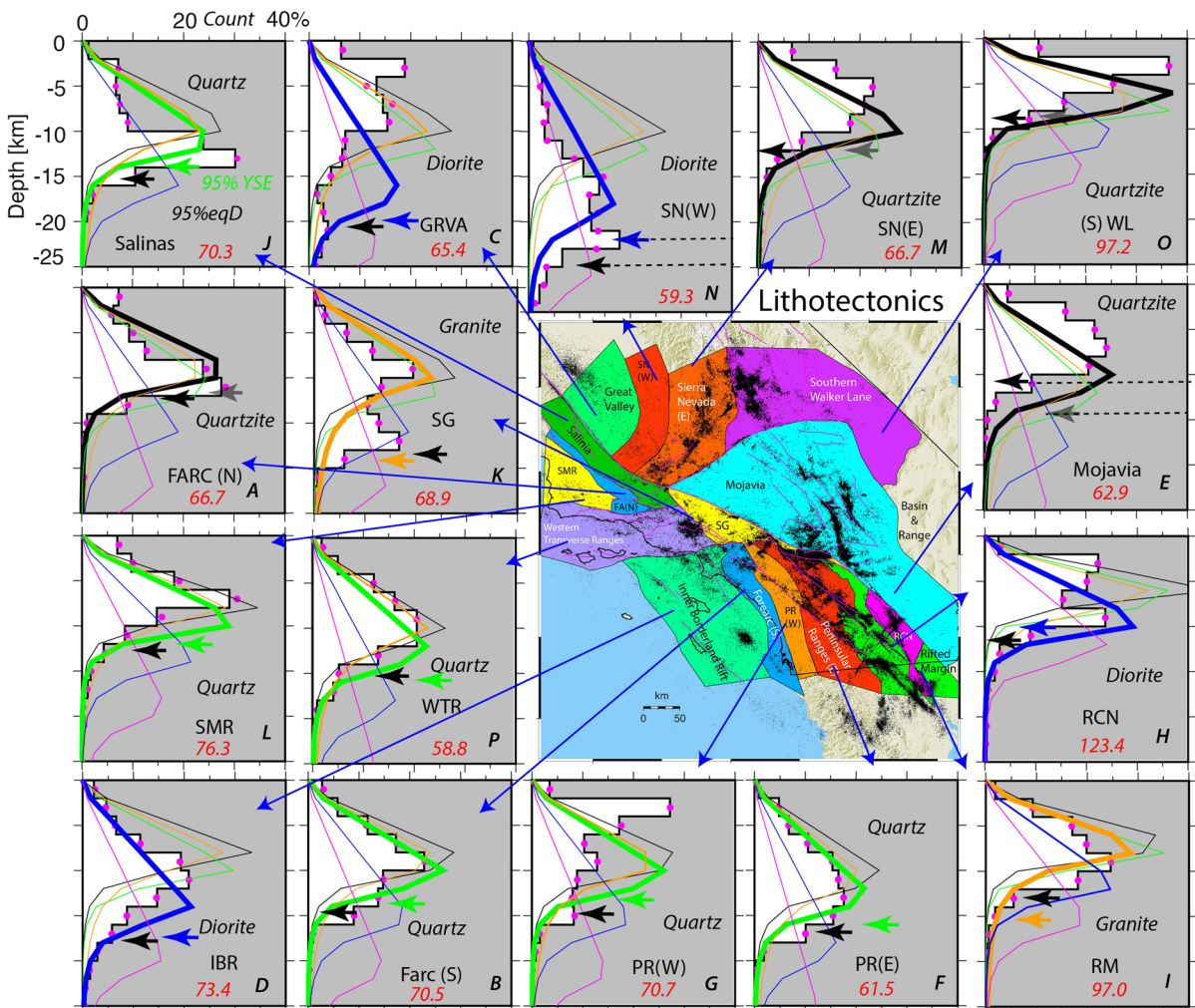


Figure 7

Relative yield strength envelopes (YSE) and earthquake depth histograms (EDH) for the 16 lithotectonic blocks in southern California. The 95%D for each EDH and YSE for each block are shown as arrows; with the 95%D for YSEs colored. The two cases with the 95Ds about ~ 3 km apart, are indicated with dashed lines. The YSEs are color coded with: Quartzite—black; Quartz—green; Granite—orange; Diorite—blue; and Mafic granulite—magenta. The average heat flow value within each block is shown as a red number in mWm^{-2} . See Table 2 and Fig. 6 for block names and labels. The letters A, B, C etc. enable cross reference to Table 2

lithologies we identify the best matching lithology as the one that produces a YSE with a 95%D depth most similar to the respective EDH 95%D.

The YSEs for the different lithologies in each block are shown in Fig. 7. In 12 out of the 16 blocks, the best matching lithologies are felsic (Granite, Quartzite or Quartz). The depth extent of seismicity in the Great Valley, the Western Sierra Nevada, the Inner Borderland Rift and the Rifted Crust North, on the other hand, is much more consistent with a dioritic lithology. There are no examples where envelopes of more dense rocks such as mafic granulite are required to fit the EDHs D95%.

One of the limitations of this modeling is the similarity of the YSEs for some lithologies. In particular, the different quartz-dominated rocks such as quartzite, quartz, and granite often have very similar YSEs, where usually one of these provides a somewhat better fit. In contrast, our best fitting YSEs differentiate clearly between the quartz versus the diorite-dominated lithologies.

The inferred lithologies are qualitatively consistent with the tectonic history and petrological composition of the blocks. Our study separates out the more dioritic (feldspar-rich) blocks, including the batholiths, ophiolite, and nascent gabbroic crust. The western Sierra Nevada and the Peninsular Ranges batholiths are parts of a Mesozoic magmatic arc and consist of complex plutons rich in mafic and tonalitic rocks (e.g., Saleeby 2003). The high-density gabbroic ophiolite crust beneath the southeastern Great Valley is interpreted as a remnant from past subduction (Fliedner et al. 2000). The crust in the Salton Trough consists of high-density gabbroic rocks with mafic intrusions, like the Salton Buttes (Barak et al. 2015; Han et al. 2016). This is in contrast to the less dense, and in some cases younger blocks that form a different thermo-mechanical and lithological group with predominantly quartz composition, such as the Salinas, western Transverse Ranges, Mojavia, and southern Walker Lane.

The inferred lithologies are also qualitatively consistent with the 3D seismic velocity models of Lee et al. (2014). At mid-crustal depths beneath the parts of the Great Valley, batholiths [Sierra Nevada (W)], the Inner continental Borderland, and Peninsular Ranges, the Lee et al. (2014) model has elevated

V_p , V_s , and V_p/V_s values. This is in agreement with the elevated values found for dioritic rocks in empirical studies (Christensen 1996; Brocher 2005). Similarly, their model has V_p , V_s , and V_p/V_s values that are below average beneath the eastern Mojave, Walker Lane, and the western Transverse Ranges. These values agree with the quartz-rich compositions we infer, which often have average or slightly lower V_p/V_s ratios because their V_p is lower than average. Thus, although the southern California geology is complex, our inferred block lithologies are consistent with independently determined regional geological considerations, and with state-of-the-art 3D velocity models.

4.3. Absolute Differential Yield Stress and Geotherm Profiles

We use the absolute differential stress and temperature depth profiles that correspond to the YSEs with the best matching lithology, to parameterize the thermo-mechanical properties of the crustal blocks (Fig. 8). These models are important for understanding the long-term crustal deformation along the Pacific-North America plate boundary as well as short-term earthquake source processes (e.g., Burgmann and Dresen 2008).

The differential stress and temperature profiles exhibit significant variability between lithotectonic blocks with the peak differential stress varying from about ~ 100 MPa at 8-km depth in hotter and more felsic crust to ~ 500 MPa at 18-km depth at greater depths for predominantly diorite crust. Three major spatial patterns in the differential stress profiles between blocks emerge. First, the blocks located to the northeast [Sierra Nevada (E), Walker Lane (s), and the Mojavia] all have felsic composition and low differential stress. Second, to the west and southwest of the San Andreas Fault [Rifted Margin, Peninsular Ranges (E & W), Forearc (S), Santa Maria rift, San Gabriel, and Salinas] the composition is felsic with two cases of granite with average differential stress. Third, parts of the Great Valley, batholiths [Sierra Nevada (W)] and the Inner continental Borderland all exhibit diorite composition and high differential stress. These variations in spatial pattern of lithology and stress are consistent with the lithotectonic model

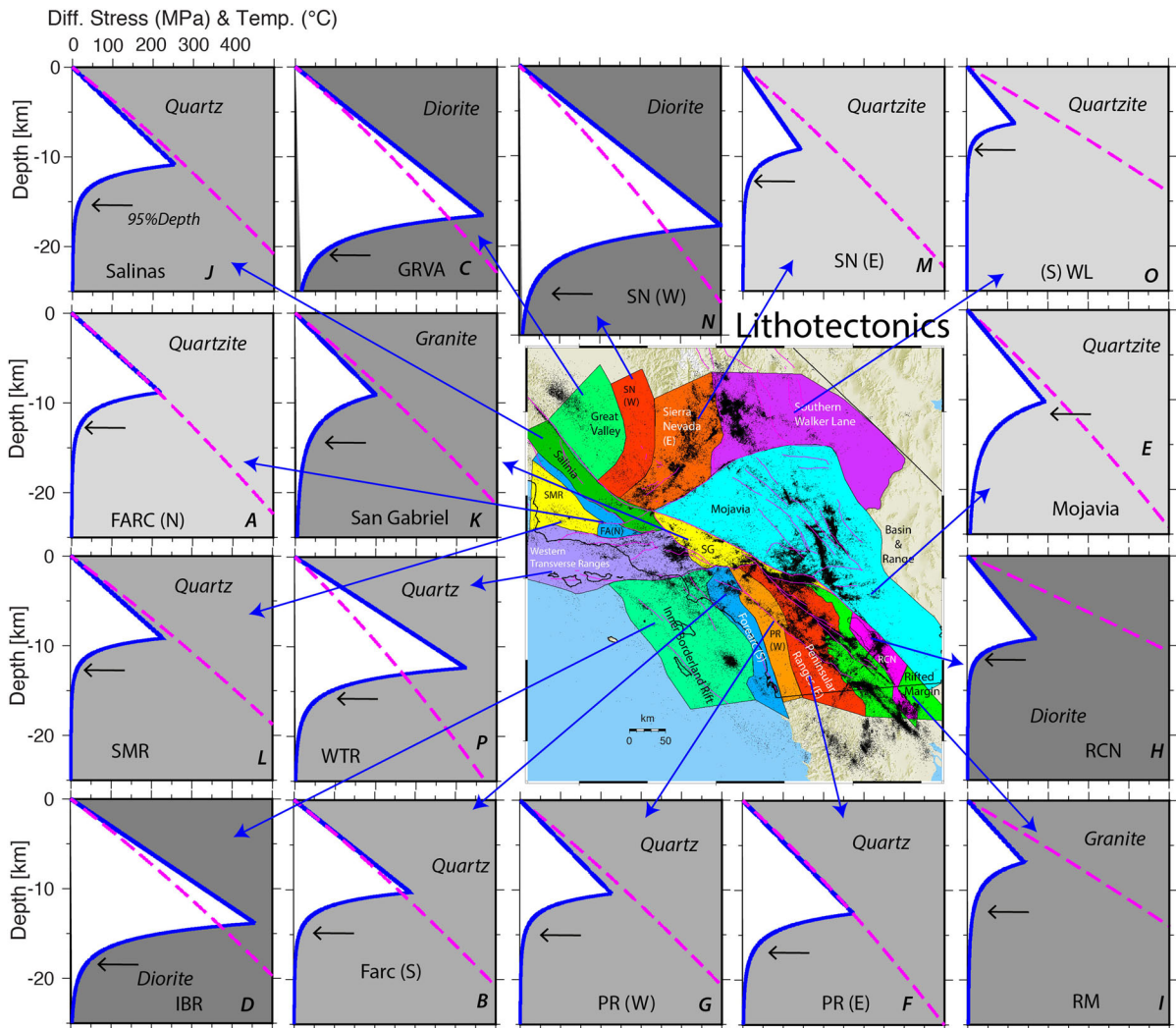


Figure 8

The differential stress and temperature plotted versus depth for the 16 lithotectonic blocks. Lithologies are indicated by background shades of gray and are also labeled. The two-layered models are also shown in Fig. 8. The dashed magenta lines represent the temperature gradient with depth. The dashed horizontal black lines represent the 95% depth of seismicity. See Fig. 6 for block names and labels

presented by Crouch and Suppe (1993), and probably not caused by uncertainties in the geothermal gradient or other geophysical parameters.

In some cases, current tectonics explain the observed differences in differential stress. In particular, there is a clear difference in differential stress between the Great Valley block and San Gabriel blocks as expected because they are separated by the San Andreas Fault, which has a large cumulative offset of 100 s of kilometers (Fig. 8). Previously, the change in stress or strength across the San Andreas Fault has been identified in stress inversion studies

(e.g., Yang and Hauksson 2013). Using geodetic data Huang and Johnson (2012) showed that the Salinas block, located on the west side of the San Andreas Fault, has a thinner and stiffer elastic thickness as compared to the Great Valley block on the east side. Their result differs from ours because our version of the Great Valley block includes the deep ophiolite to the east. Similarly, Bird (2017) pointed out the stress guide effects of the Peninsular Ranges and Sierra Nevada batholiths as they accommodate high stress and low strain as opposed to low stress and high strain along the tectonically active plate boundary.

Table 2
Mean values of geophysical parameters for each lithotectonic block

Lithotectonic block	ID ^c	Event based heatflow ^a [mW/m ²]	Strain rate [s ⁻¹] 10 ⁻¹⁵	Style of faulting	# of quakes	Model lithology	Seism. D95% depth [km]	Temp at seis 95%D °C	Litho. D95% depth [km]	C & S 1993 ^b lithology
Forearc										
Forearc (N)	A	66.7	2.8	1.6	193	Quartzite	12.5	297	12.0	GV franciscan sequence
Forearc (S)	B	70.5	5.0	1.8	4771	Quartz	14.5	362	13.1	GV franciscan sequence
Transverse ranges (W)	P	58.8	5.5	2.2	22,641	Quartz	15.4	310	15.7	GV franciscan sequence
Rifts										
Inner borderland	D	73.4	3.3	2.0	5642	Diorite	17.7	453	17.2	Schist/igneous rocks
Rifted crust (N)	H	123.4	19.5	1.1	30,133	Diorite	12.0	559	11.6	Granitic batholith
Rifted margin	I	97.0	9.0	1.3	58,184	Granite	12.5	449	15.2	Granitic batholith
Santa maria rift	L	76.3	2.1	1.6	462	Quartz	12.6	348	11.6	Schist/igneous rocks
(S) walker lane	O	97.2	2.9	1.2	88,293	Quartzite	8.7	319	8.8	Granitic batholith
Terrane										
Mojave	E	62.9	7.0	1.2	119,937	Quartzite	11.0	248	14.1	Granitic batholith
Salina	J	70.3	9.2	1.5	1109	Quartz	15.2	377	13.7	Granitic batholith
San Gabriel	K	68.9	7.2	1.4	27,655	Granite	17.8	424	19.1	Schist/granitic batholith
Rigid Block										
Great valley	C	65.4	6.7	1.7	872	Diorite	21.2	466	20.5	GV sequence/ ophiolite
Batholith										
Sierra Nevada (E)	M	66.7	1.9	1.0	42,377	Quartzite	12.5	297	12.7	Granitic batholith
Sierra Nevada (W)	N	59.3	2.7	1.7	580	Diorite	24.9	476	22.0	Metamorphic belt/ ophiolite
Peninsular ranges (E)	F	61.5	8.0	1.4	104,702	Quartz	16.7	351	15.8	Granitic batholith
Peninsular ranges (W)	G	70.7	4.0	1.4	4124	Quartz	14.8	370	13.2	Metamorphic schist/ volcanics

^aAverage heat flow derived from heat flow values at each epicenter; from USGS data

^bC&S 1993 refers to Crouch and Suppe (1993)

^cReference block identifier (ID) letter also used in Figs. 6, 7, 8, and 9

Overall, our results agree with previous studies that showed the transition from brittle to ductile regime depends on lithology with $300^\circ \pm 50^\circ \text{C}$ for quartz-rich rocks, $450^\circ \pm 100^\circ \text{C}$ for feldspar-rich diorite rocks, and $650^\circ \pm 100^\circ \text{C}$ for olivine rich rocks (e.g. Sibson 1983; Magistrale and Zhou 1996; Ranalli 1997; Bonner et al. 2003).

4.4. Crustal Thermo-mechanics

To synthesize the overall thermo-mechanical properties, we analyze the geophysical crustal parameters at the D95% depth of seismicity: (1) the D95% depth of the YSE, (2) predicted temperature, and (3) peak differential stress (Fig. 9). All of these

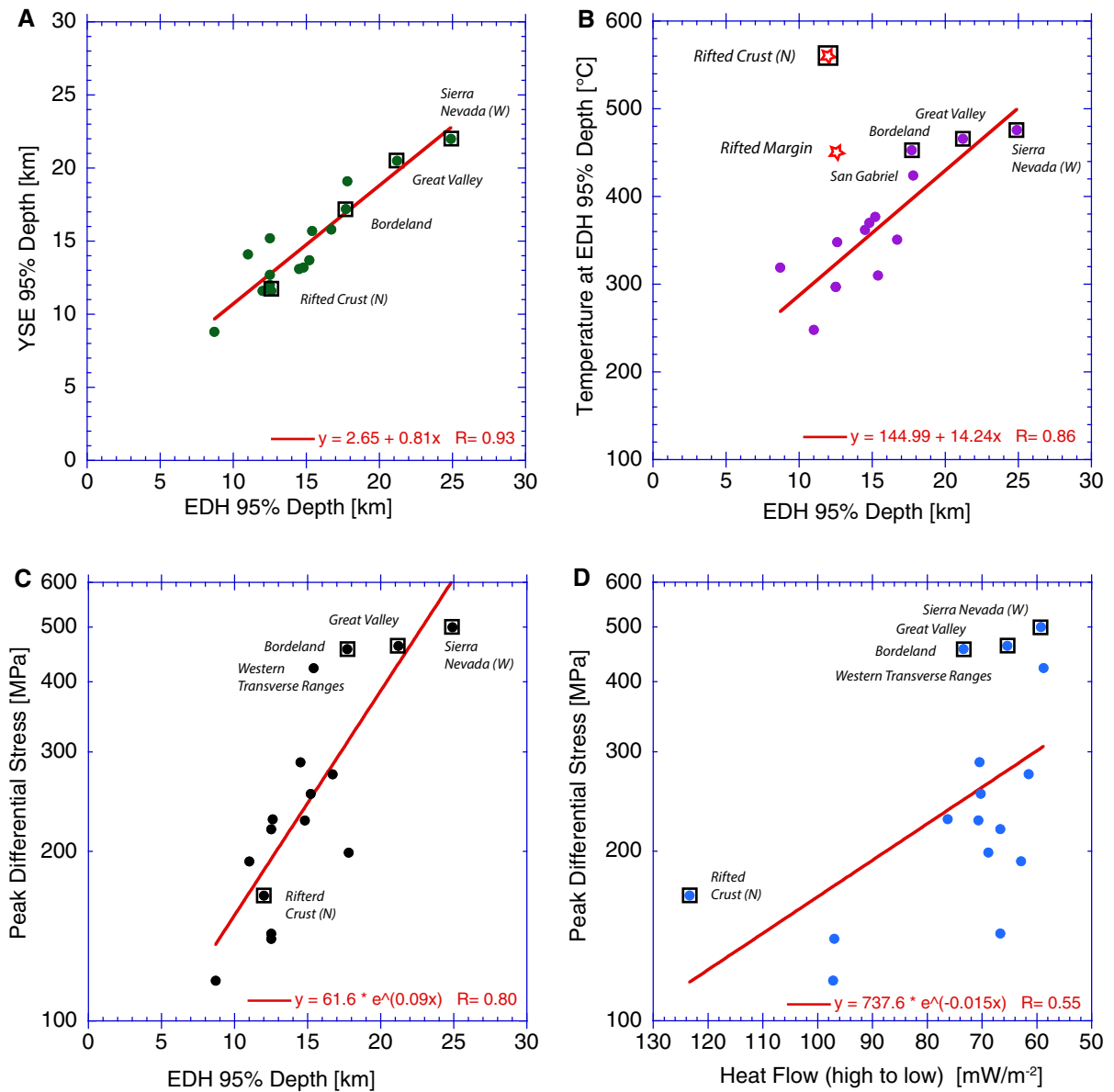


Figure 9

Comparison of geophysical crustal parameters. The data points for the four diorite blocks are labeled and marked as with black squares. A few other data points of special interest are also labeled. The red line shows a linear or exponential fit as calculated with the included formula; the correlation factor, *R* is also shown. **a** Preferred YSE 95% depth versus EDH 95% depth. **b** The estimated temperature at the EDH 95%D versus the corresponding EDH 95%D. Two anomalous data points that did not fit the regression curve are shown as red stars, Rifting Crust North, and Rifting Margin. Both cover parts of the Salton Trough suggesting that heat flow is overestimated where the seismicity is occurring. In **c** and **d**, logarithm of peak differential stress versus **c** EDH 95%D and **d** heat flow plotted from high to low values

parameters exhibit significant variations with values of the EDH 95%D for different blocks. We also compare the heat flow to the corresponding peak differential stress. We used solid circle symbols except for the blocks of diorite composition, which we overlay by a square symbol.

As expected, the lithology 95%D and seismicity 95%D are well correlated with a regression coefficient of 0.93 as shown in Fig. 9a. The seismicity 95%D increases in depth about 19% faster than the lithology 95%D, which is in part expected from the denser and colder diorite lithology.

There are some uncertainties in each temperature profile depending on local variations in the heat flow and the radiogenic heat production at depth, but nonetheless we observe significant differences between lithologies (Fig. 9b). The quartz composition dominated blocks range in temperature from ~ 100 to ~ 300 °C at depths ranging from 9 to 18 km. In comparison, the peak temperatures in diorite rich blocks are close to 500 °C except for the Rifted Crust north, which peaks at ~ 550 °C. The temperature profiles reach $500^\circ \pm 50$ °C at depths ranging from 10 to 26 km, which is considered to be the maximum temperature where crustal earthquakes can occur.

The seismicity 95%D could be shallower or deeper in limited regions if the tectonic strain rate varies more than predicted by the geodetic model used in this study. For instance, Takeuchi and Fialko (2012) argued that viscous heating in shear zones that are several kilometers wide and may sustain a temperature anomaly of 200–400 °C. The data that are shown in Fig. 9b show such anomalously high temperatures only within the Rifted Margin and Rifted Crust (*N*) blocks. Alternatively, this anomalous temperature could be caused by the heat flow being overestimated where the seismicity occurs within these blocks. By smoothing the heat flow in the Salton Trough, we smear the very high heat flow anomalies in the geothermal areas into the surrounding regions, which are like to have much lower heat flow and a steeper temperature gradient.

The peak differential stress increases with the seismicity cutoff 95%D consistent with its dependence on combined effects of temperature and lithology with depth (Fig. 9c). Three of the four diorite blocks and the Transverse Ranges block accommodate the highest stresses. When ignoring the depth dependence of the differential stress, and only investigating the heat flow dependence, the same four blocks have consistently high stress and low heat flow. The anomalous diorite Rifted Crust North that exhibits the highest heat flow, probably has its heat flow overestimated by at least 30% as discussed above (Fig. 9d).

Apart from pore pressures, the parameters affecting the decay of the YSEs and EDHs at depth are known from field or laboratory observations. The

differential stress profiles may be upper bound estimates if high fluid pressures exist (higher than the hydrostatic assumed here) because these may lower the effective strength (e.g., Sibson, 1974). However, any strength reduction caused by fluids may be more important at shallow depths where effective contact areas on faults are small, than at large depths, and where creep or slow plastic deformation increases the effective contact area (Hirth and Beeler, 2015).

In summary, the peak differential stress is small for shallow seismicity in high heat flow regions such as Rifted Crust north, and large for deep seismicity in low heat flow regions, such as Sierra Nevada west. The change in block lithology from predominantly quartz- to feldspar-rich diorite increase the depth range of the seismicity by 7 km or down to maximum block averaged depth of 26 km. This is consistent with the 95%D of the pairs of EDHs and YSEs representing the transition zone where there is rapid decrease in strength, stressing rate, and availability of nucleations.

5. Discussion

Our thermo-mechanical model consists of depth profiles of absolute differential stress, temperature, and lithology of each block. This model is a step towards improved understanding of the constitutive relations that control the long-term tectonic deformation of southern California. It shows peak differential stresses that the crustal material in each block can possibly withstand, ranging from low ~ 150 MPa to very high ~ 500 MPa. Locally the earthquakes are occurring under these stress conditions, which also correspond to the local yield strength of the rocks. The limitations of the model include various averaging of geophysical variables as well as scarce knowledge of the presence of fluids and deformation processes in the lower crust. Below, we discuss the model limitations and compare the model to independent models of absolute crustal stress in southern California.

5.1. *Effects of Heat Flow and, Strain Rate*

Regional variations in both heat flow and tectonic strain rate affect the details of the thermo-mechanical model but style of faulting has a much smaller effect. The heat flow that is a proxy for the temperature gradient with depth exhibits gradual spatial variations across the plate boundary region. In contrast, the tectonic strain rates are usually concentrated along major faults but facilitate some scattered seismicity across the region.

In general, our model that is based on minimizing the difference between the EDH and YSE 95%D values is consistent with the general results from previous studies that reported onset of plasticity in schist rocks of quartz and micas at $\sim 260 \pm 40$ °C, while feldspar-rich rocks become ductile at $\sim 450 \pm 50$ °C (e.g., Sibson 1982; Bonner et al. 2003). Our model also agrees with Magistrale and Zhou (1996) who argued that this variability in the composition of rocks caused 4–10 km changes in depth to the base of the seismicity. They showed that areas inferred to be underlain by schist rocks had shallower seismicity than areas possibly floored by basement rocks with higher feldspar content. In a later study, Magistrale (2002) concluded that heat flow and lithology affected similarly the depth distribution of earthquakes in southern California, which is also confirmed by our study.

The largest mismatch between the 95%D values is observed in the Mojave Desert where the seismicity is shallower than expected from the measured heat flow and strain rates (Fig. 7), for all the possible lithologies. Previously Williams (1996) showed that the heat flow varied from ~ 50 mWm⁻² in the south to 70 mWm⁻² in the north along the 1992 Joshua Tree and Landers ruptures. We used an average heat flow of 62.9 mWm⁻² for the whole Mojave block but a value of 70 mWm⁻² would raise the YSEs by 2–3 km, and thus make the EDH and the YSE more consistent. Thus we infer that the heat flow in the Mojave may be underestimated. For instance, regional aquifers beneath the Mojave Desert may perturb the surficial heat flow measurements. The heat flow in the Sierra Nevada west block where the 95%D values also differ may be overestimated by a similar amount

because of the difficulty in finding suitable measurement sites.

The geodetically measured tectonic strain field is explicitly accounted for in the determination of the thermo-mechanical profiles or the YSEs. In a complementary approach, Smith-Konter et al. (2011) determined the depth of the seismogenic zone by treating the locking depth estimates from both geodetic and seismological data independently. They found consistent geodetic locking depths of 6–22 km and 95% seismicity cutoff depths of 11–20 km, which agrees with the 95%D estimates in this study. In one case, they found inconsistent locking depths in the Salton Trough region with much shallower geodetically inferred locking depths on fault segments as compared to the local EDHs. In contrast, we find a good match between the EDH and YSE for the Salton Trough when assuming diorite lithology, which is consistent with geological observations (Mooney and Weaver 1989).

5.2. *Absolute Crustal Stress Field*

In general, the crustal stress field consists of three main components: lithostatic pressure load, topographic stress deviations related to lithological density variations, and tectonic stress variations (Bird 2017). Our study provides a model of the differential stress field as a function of depth for each block by averaging lateral variations within blocks. The variations with depth in each block and between blocks reflect the regional tectonic stress variations, but smooth out variations near major fault zones (Takeuchi and Fialko 2012). The average crustal stress field determined with our block approach is consistent with the results of Townend and Zoback (2000) who argued that in general crustal strength is maintained by critically stressed faults with hydrostatic pore pressure.

Our model is consistent with the absolute stress field in the southern California crust as determined by Bird (2017) who showed that low heat flow regions are strong and act as stress guides with a very low long-term strain rate. In contrast, areas of elevated or high heat flow are characterized by low stresses and high long-term strain rate, often expressed by faults with high slip rate. We find similar high differential

stresses within the low heat flow and low strain rate Sierra Nevada and Peninsular Ranges batholiths and low stresses in areas of elevated heat flow and strain rate, such as the Salton Trough. The eastern Sierra Nevada seismicity exhibits similar behavior as the off-plate boundary seismicity found in northern California, to the east of the San Andreas Fault, away from the plate boundary (Miller and Furlong 1988). In particular, the off-plate boundary region beneath the Sierra Nevada that has a large crustal thickness of 37–43 km is floored by seismicity with a cutoff depth at ~ 250 °C (Hauksson 2011).

In a recent study, Luttrell and Smith-Konter (2017) determined absolute differential stresses in the southern California crust by balancing topographic stresses and stress orientations from focal mechanisms. They argued that at seismogenic depths, the stresses were larger than 62 MPa at ~ 5 -km depth and that pore pressures were probably close to hydrostatic with average coefficient of friction. We find a much wider range in average differential stress levels, extending up to ~ 150 MPa at 5-km depth. In general, the peak differential stress varies significantly both in value and depth between blocks (Fig. 9). We do not find an obvious lower differential stress limit for driving seismicity, but our results are consistent with those of Luttrell and Smith-Konter (2017) who identified 20 MPa as the minimum differential stress required to drive the stressing rate causing seismicity.

5.3. Block Models and Their Limitations

Our approach of analyzing the thermo-mechanics of lithotectonic blocks provides regional parameters for geodynamic models. The thermo-mechanics of the blocks describes how they respond to long-term tectonic deformation as they participate in the strain loading and release over the numerous earthquake cycles. Our results are compatible with the results of Chéry (2008) who analyzed regional variations of the elastic thickness of the crust, which included several strike-slip faults. He showed that the regional elastic thickness played a major role in determining the strength of faults within blocks. In contrast most previous studies have focused on modeling the rheology of thin fault zones as 1D or 2D structures.

These studies usually provide only information about the specific fault and assume the same rheology of the blocks on either side (e.g., Thatcher and England 1998). In this study we implicitly assume that the major faults are locked and determine the thermo-mechanics of the blocks that are in many cases bounded by major faults such as the San Andreas Fault.

The shapes of the EDHs can be affected by localized variations in heat flow or the stressing rate that may not be captured in our analysis. In regions with very high heat flow geothermal areas, the smoothed regional heat flow may be overestimated, and earthquakes are actually occurring at lower temperatures than suggested by our model. Similarly, small-scale variations in the stressing rate in the ductile zone can modulate seismicity rates within the upper brittle layer (Sammis et al. 2016) but our block averaging may minimize these effects. Because > 30 Ma have passed since these lithotectonic blocks were formed, their stress and temperature profiles are likely to have been overprinted several times. Thus, we do not expect a simple extrapolation of stress and temperature between blocks. These, as well as other model limitations, may affect the differential stress, temperature, and lithology profiles but calculating formal uncertainties is beyond the scope of this paper.

6. Conclusions

The long-term thermo-mechanical properties of the crust vary across the southern California plate boundary. To map these variations, we minimize the depth offset of EDHs and YSEs near their respective cutoff 95%D depths, and determine a best matching average lithology for each of the 16 lithotectonic blocks. In general the inferred lithology is mostly of quartz-rich composition within only four blocks out of 16 of predominantly feldspar-rich diorite composition, and consistent with the tectonic history of the blocks.

In agreement with previous studies, the absolute differential stress profiles derived from the forward modeling of the EDHs show a general pattern of high differential stresses within the low heat flow Sierra Nevada and Peninsular Ranges batholiths and low

stresses in areas of elevated heat flow, such as the Salton Trough. We find highly variable average differential stress levels between blocks, extending up to ~ 500 MPa, and the depth of the stress peak varies significantly between blocks. Within the diorite-dominated crustal blocks the lithology is colder and denser, and the differential peak stress is deeper and larger.

Acknowledgements

We thank J.-P. Avouac, N. Beeler, L. M. Jones, J. P. Ampuero, N. van der Elst, and J. Stock for discussions; J. Albaric for sharing her matlab code for calculating the YSEs, and Z. Ross for the declustered catalog. This research was supported by USGS/NEHRP grants G16AP00147 & G18AP00028; NSF award: EAR-1550704; and by the Southern California Earthquake Center, which is funded by NSF Cooperative Agreement EAR-1033462 and USGS Cooperative Agreement G12AC20038. This paper is SCEC contribution # 8085. We used GMT from Wessel et al. (2013) to make the Figures. We have used waveforms and parametric data from the Caltech/USGS Southern California Seismic Network (SCSN); <https://doi.org/10.7914/sn/ci>; stored at the Southern California Earthquake Data Center. <https://doi.org/10.7909/c3wd3xh1>.

REFERENCES

- Afonso, J. C., & Ranalli, G. (2004). Crustal and mantle strengths in continental lithosphere: is the jelly sandwich obsolete? *Tectonophysics*, 394, 221–232.
- Albaric, J., Déverchère, J., Petit, C., Perrot, J., & Le Gall, B. (2009). Crustal rheology and depth distribution of earthquakes: insights from the central and southern East African rift system. *Tectonophysics*, 468, 28–41. <https://doi.org/10.1016/j.tecto.2008.05.021>.
- Barak, S., Klemperer, S. L., & Lawrence, J. F. (2015). San andreas fault dip, peninsular ranges mafic lower crust and partial melt in the Salton trough, Southern California, from ambient-noise tomography. *Geochemistry, Geophysics, Geosystems*, 16, 3946–3972. <https://doi.org/10.1002/2015GC005970>.
- Beeler, N. M., Hirth, G., Tullis, T. E. & Webb, C. H. (2018). On the depth extent of coseismic rupture. *Bulletin of the Seismological Society of America*, 108(2), 761–780.
- Ben-Zion, Y., & Lyakhovskiy, V. (2006). Analysis of aftershocks in a lithospheric model with seismogenic zone governed by damage rheology. *Geophysical Journal International*, 165(1), 197–210. <https://doi.org/10.1111/j.1365-246X.2006.02878.x>.
- Bird, P. (2017). Stress field models from Maxwell stress functions: southern California. *Geophysical Journal International*, 210, 951–963. <https://doi.org/10.1093/gji/ggx207>.
- Bonner, J. L., Blackwell, D. D., & Herrin, E. T. (2003). Thermal constraints on earthquake depths in California. *Bulletin of the Seismological Society of America*, 93, 2333–2354. <https://doi.org/10.1785/0120030041>.
- Brocher, T. M. (2005). Empirical relations between elastic wave-speeds and density in the earth's crust. *Bulletin of the Seismological Society of America*, 95(6), 2081–2092. <https://doi.org/10.1785/0120050077>.
- Burgmann, R., & Dresen, G. (2008). Rheology of the lower crust and upper mantle: evidence from rock mechanics, geodesy, and field observations. *Annual Review of Earth and Planetary Sciences*, 36(1), 531–567. <https://doi.org/10.1146/annurev.earth.36.031207.124326>.
- Burov, E. B. (2011). Rheology and strength of the lithosphere. *Marine and Petroleum Geology*. <https://doi.org/10.1016/j.marpetgeo.2011.05.008>.
- Byerlee, J. D. (1967). Frictional characteristics of granite under high confining pressure. *Journal of Geophysical Research*, 72, 3639–3648.
- Chapman, A. D. (2017). The Pelona–Orocopia–Rand and related schists of southern California: a review of the best-known archive of shallow subduction on the planet. *International Geology Review*, 59(5–6), 664–701. <https://doi.org/10.1080/00206814.2016.1230836>.
- Chéry, J. (2008). Geodetic strain across the San Andreas fault reflects elastic plate thickness variations (rather than fault slip rate). *Earth and Planetary Science Letters*, 269(3–4), 352–365.
- Christensen, N. I. (1996). Poisson's ratio and crustal seismology. *Journal of Geophysical Research*, 101(B2), 3139–3156.
- Crouch, J. K., & Suppe, J. (1993). Late cenozoic tectonic evolution of the Los Angeles basin and inner California borderland: a model for core complex-like crustal extension. *GSA Bulletin*, 105(11), 1415–1434. [https://doi.org/10.1130/0016-7606\(1993\)105<1415:LCCTEOT>2.3.CO;2](https://doi.org/10.1130/0016-7606(1993)105<1415:LCCTEOT>2.3.CO;2).
- Déverchère, J., Petit, C., Gileva, N., Radziminovitch, N., Melnikova, V., & San'kov, V. (2001). Depth distribution of earthquakes in the Baikal rift system and its implications for the rheology of the lithosphere. *Geophysical Journal International*, 146, 714–730.
- Doser, D. I., & Kanamori, H. (1986). Depth of seismicity in the imperial valley region (1997–1983) and its relationship to heat flow, crustal structure, and the October 15, 1979, earthquake. *Journal of Geophysical Research*, 91, 675–688. <https://doi.org/10.1029/JB091iB01p00675>.
- Fliedner, M. M., Klemperer, S. L., & Christensen, N. I. (2000). Three-dimensional seismic model of the Sierra Nevada arc, California, and its implications for crustal and upper mantle composition. *Journal of Geophysical Research*, 105(B5), 10899–10921. <https://doi.org/10.1029/2000JB900029>.
- Han, L., Hole, J. A., Stock, J. M., Fuis, G. S., Kell, A., Driscoll, N. W., et al. (2016). Continental rupture and the creation of new crust in the Salton trough rift, Southern California and northern Mexico: results from the salton seismic imaging project. *Journal of Geophysical Research*, 121(10), 7469–7489.
- Harden, D. R. (1998). *California Geology*, Upper Saddle River, NJ: Prentice-Hall Inc., pp. 479. ISBN 0-02-350042-5.

- Hauksson, E. (2011). Crustal geophysics and seismicity in southern California. *Geophysical Journal International*, 186, 82–98. <https://doi.org/10.1111/j.1365-246X.2011.05042.x>.
- Hauksson, E., Yang, W., & Shearer, P. M. (2012). Waveform relocated earthquake catalog for Southern California (1981 to June 2011). *Bulletin of the Seismological Society of America*, 102(5), 2239–2244. <https://doi.org/10.1785/0120120010>.
- Hirth, G., & Beeler, N. M. (2015). The role of fluid pressure on frictional behavior at the base of the seismogenic zone. *Geology*, 43, 223–226.
- Holt, W. E., Klein, E. & Flesch, L. M. (2010). GPS strain rates, optimal fault slip rates, and predicted moment rates in Western U.S. Plate Boundary Zone, In *Proceedings of the Workshop on Incorporating Geodetic Surface Deformation Data into UCERF3*, Palm Spring, California. <https://files.scec.org/s3fs-public/AgendaAbstracts.pdf>. Accessed 21 Aug 2018.
- Huang, W.-J., & Johnson, K. M. (2012). Strain accumulation across strike-slip faults: investigation of the influence of laterally varying lithospheric properties. *Journal of Geophysical Research*, 117, B09407. <https://doi.org/10.1029/2012JB009424>.
- Jacobson, C. E., Grove, M., Pedrick, J. N., Barth, A. P., Marsaglia, K. M., Gehrels, G. E., et al. (2011). Late cretaceous to early cenozoic tectonic evolution of the southern California margin inferred from provenance of trench and forearc sediments. *Geological Society of America Bulletin*, 123(3–4), 485–506. <https://doi.org/10.1130/B30238.1>.
- Jennings, C. W., & W. A. Bryant (2010). Fault activity map of California. Geologic Data Map No. 6, California Geological Survey, Sacramento, California, US. <http://maps.conservation.ca.gov/cgs/fam/>. Accessed 21 Aug 2018.
- Lee, E.-J., Chen, P., Jordan, T. H., Maechling, P. B., Denolle, M. A. M., & Beroza, G. C. (2014). Full-3-D tomography for crustal structure in Southern California based on the scattering-integral and the adjoint-wavefield methods. *Journal of Geophysical Research: Solid Earth*, 119, 6421–6451. <https://doi.org/10.1002/2014JB011346>.
- Luttrell, K., & Smith-Konter, B. (2017). Limits on crustal differential stress in southern California from topography and earthquake focal mechanisms. *Geophysical Journal International*, 211(1), 472–482. <https://doi.org/10.1093/gji/ggx301>.
- Luyendyk, B. P., Kamerling, M. J., & Terres, R. R. (1980). Geometric model for neogene crustal rotations in southern California. *Geological Society of America Bulletin*, 91, 211–217.
- Magistrale, H. (2002). Relative contributions of crustal temperature and composition to controlling the depth of earthquakes in Southern California. *Geophysical Research Letters*, 29(10), 1447. <https://doi.org/10.1029/2001GL014375>.
- Magistrale, H., & Zhou, H. (1996). Lithologic control of the depth of earthquakes in Southern California. *Science*, 273, 639–642. <https://doi.org/10.1126/science.273.5275.639>.
- Mahan, K. H., Guest, B., Wernicke, B., & Niemi, N. A. (2009). Low-temperature thermochronologic constraints on the kinematic history and spatial extent of the Eastern California shear zone. *Geosphere*, 5(6), 483–495. <https://doi.org/10.1130/GES00226.1>.
- Matti J. C., & Morton D. M. (1993). Paleogeographic evolution of the San Andreas Fault in southern California: a reconstruction based on a new cross-fault correlation: In R. E. Powell, R. J. Weldon, II & J. C. Matti (Eds.), *The San Andreas Fault system: displacement, palinspastic reconstruction, and geologic evolution*. Geological Society of America, Memoir 178 (Chapter 2, special volume, pp. 107–160). Geological Society of America.
- Miller, C. K., & Furlong, K. P. (1988). Thermal-mechanical controls on seismicity depth distributions in the San Andreas fault zone. *Geophysical Research Letters*, 15, 1429–1432. <https://doi.org/10.1029/GL015i012p01429>.
- Miller, J. S., Glazner, A. F., Farmer, G. L., Suayah, I. B., & Keith, L. A. (2000). A Sr, Nd, and Pb isotopic study of mantle domains and crustal structure from miocene volcanic rocks in the Mojave Desert, California. *Geological Society of America Bulletin*, 112, 1264–1279. [https://doi.org/10.1130/00167606\(2000\)112<1264:ASNAPI>2.0.CO;2](https://doi.org/10.1130/00167606(2000)112<1264:ASNAPI>2.0.CO;2).
- Mooney, W., & Weaver, C. (1989). Regional crustal structure and tectonics of the Pacific coastal states; California, Oregon, and Washington. In L. Pakiser & W. Mooney (Eds.), *Geophysical framework of the continental United States GSA memoir 172* (pp. 129–162). Boulder: Geological Society of America.
- Nazareth, J. J., & Hauksson, E. (2004). The seismogenic thickness of the Southern California crust. *Bulletin of the Seismological Society of America*, 94, 940–960. <https://doi.org/10.1785/0120020129>.
- Oskin, M. E., Behr, W. M., Hearn, L., & Thatcher, W. (2016). Community Rheology model workshop: establishing a geologic framework. Southern California Earthquake Center (SCEC), workshop report, Los Angeles, CA. <https://www.scec.org/proposal/report/16183>. Accessed 21 Aug 2018.
- Putirka, K., Jean, M., Cousens, B., Sharma, R., Torrez, G., & Carlson, C. (2012). Cenozoic volcanism in the sierra Nevada and walker lane, California, and a new model for lithosphere degradation. *Geosphere*, 8(2), 265–291. <https://doi.org/10.1130/GES00728.1>.
- Ranalli, G. (1997). Rheology and deep tectonics. *Annals of Geophysics*, 40(3), 671–680.
- Rolandone, F., Bürgmann, R., & Nadeau, R. M. (2004). The evolution of the seismic- aseismic transition during the earthquake cycle: constraints from the time- dependent depth distribution of aftershocks. *Geophysical Research Letters*, 31, L23610. <https://doi.org/10.1029/2004GL021379>.
- Saleeby, J. (2003). Production and loss of high-density batholithic root, southern Sierra Nevada, California. *Tectonics*, 22(6), 1064. <https://doi.org/10.1029/2002TC001374>.
- Sammis, C. G., Smith, S. W., Nadeau, R. M., & Lippoldt, R. (2016). Relating transient seismicity to episodes of deep creep at Parkfield, California. *BSSA*, 106(4), 1887–1899. (225).
- Sass, J. H., Williams, C. F., Lachenbruch, Arthur H., Galanis, S. P., Jr., & Grubb, F. V. (1997). Thermal regime of the San Andreas fault near Parkfield, California. *Journal of Geophysical Research*, 102(B12), 27575–27585.
- Shearer, P. M. (2002). Parallel fault strands at 9-km depth resolved on the imperial fault, Southern California. *Geophysical Research Letters*, 29(14), 19–19–4. <https://doi.org/10.1029/2002gl015302>.
- Shinevar, W. J., Behn, M. D., & Hirth, G. (2015). Compositional dependence of lower crustal viscosity. *Geophysical Research Letters*, 42, 8333–8340. <https://doi.org/10.1002/2015GL065459>.
- Sibson, R. H. (1974). Frictional constraints on thrust, wrench and normal faults. *Nature*, 249(5457), 542–544. <https://doi.org/10.1038/249542a0>. (1035).
- Sibson, R. H. (1982). Fault zone models, heat flow, and the depth distribution of earthquakes in the continental crust of the United States. *Bulletin of the Seismological Society of America*, 72(1), 151–163.
- Sibson, R. H. (1983). Continental fault structure and the shallow earthquake source. *Journal of the Geological Society*, 140(5), 741–767. <https://doi.org/10.1144/gsjgs.140.5.0741>.

- Sibson, R. H. (1984). Roughness at the base of the seismogenic zone: contributing factors. *Journal of Geophysical Research*, 89, 5791. <https://doi.org/10.1029/JB089iB07p05791>.
- Smith-Konter, B. R., Sandwell, D. T., & Shearer, P. (2011). Locking depths estimated from geodesy and seismology along the San Andreas fault system: implications for seismic moment release. *Journal of Geophysical Research*, 116, B06401. <https://doi.org/10.1029/2010JB008117>.
- Takeuchi, C. S., & Fialko, Y. (2012). Dynamic models of interseismic deformation and stress transfer from plate motion to continental transform faults. *Journal of Geophysical Research*, 117, B05403. <https://doi.org/10.1029/2011JB009056>.
- Thatcher, W., & England, P. C. (1998). Ductile shear zones beneath strikeslip faults: implications for the thermomechanics of the San Andreas fault zone. *Journal of Geophysical Research*, 103, 891–905. <https://doi.org/10.1029/97JB02274>.
- Townend, J., & Zoback, M. D. (2000). How faulting keeps the crust strong. *Geology*, 28(5), 399–402.
- Turcotte, D. L., & Schubert, G. (2002). *Geodynamics* (2nd ed., p. 456). Cambridge, New York, Melbourne: Cambridge University Press. ISBN:0-521-66186-2.
- Wessel, P., Smith, W. H. F., Scharroo, R., Luis, J. F., & Wobbe, F. (2013). Generic mapping tools: improved version released. *Eos, Transactions American Geophysical Union*, 94(45), 409–410.
- Williams, C. F. (1996). Temperature and the seismic/aseismic transition: observations from the 1992 landers earthquake. *Geophysical Research Letters*, 23, 2029–2032. <https://doi.org/10.1029/96GL02066>.
- Yang, W., & Hauksson, E. (2013). The tectonic crustal stress field and style of faulting along the Pacific North America plate boundary in Southern California. *Geophysical Journal International*, 194(1), 100–117. <https://doi.org/10.1093/gji/ggt113>.
- Zaliapin, I., & Ben-Zion, Y. (2013). Earthquake clusters in southern California I: identification and stability. *Journal of Geophysical Research: Solid Earth*, 118(6), 2847–2864.

(Received March 26, 2018, revised August 16, 2018, accepted August 20, 2018, Published online September 3, 2018)